



## Article

# (–)-Naringenin 4',7-dimethyl Ether Isolated from *Nardostachys jatamansi* Relieves Pain through Inhibition of Multiple Channels

Ru-Rong Gu <sup>1,2,†</sup>, Xian-Hua Meng <sup>3,†</sup> , Yin Zhang <sup>2,†</sup>, Hai-Yan Xu <sup>2</sup>, Li Zhan <sup>2</sup>, Zhao-Bing Gao <sup>1,2,4,5,\*</sup>, Jun-Li Yang <sup>3,\*</sup> and Yue-Ming Zheng <sup>2,\*</sup> 

<sup>1</sup> School of Chinese Materia Medica, Nanjing University of Chinese Medicine, Nanjing 210023, China; 20190883@njucm.edu.cn

<sup>2</sup> Center for Neurological and Psychiatric Research and Drug Discovery, Shanghai Institute of Materia Medica, Chinese Academy of Sciences, Shanghai 201203, China; yinz1304613@163.com (Y.Z.); hyxu@simm.ac.cn (H.-Y.X.); zhanli@simm.ac.cn (L.Z.);

<sup>3</sup> CAS Key Laboratory of Chemistry of Northwestern Plant Resources and Key Laboratory for Natural Medicine of Gansu Province, Lanzhou Institute of Chemical Physics, Chinese Academy of Sciences, Lanzhou 730000, China; mengxianhua@licp.cas.cn

<sup>4</sup> Zhongshan Institute of Drug Discovery, Institution for Drug Discovery Innovation, Chinese Academy of Sciences, Zhongshan 528400, China

<sup>5</sup> University of Chinese Academy of Sciences, No. 19A Yuquan Road, Beijing 100049, China

\* Correspondence: zbgao@simm.ac.cn (Z.-B.G.); yangjl@licp.cas.cn (J.-L.Y.); zhengyueming@simm.ac.cn (Y.-M.Z.)

† These authors contributed equally to this work.



**Citation:** Gu, R.-R.; Meng, X.-H.; Zhang, Y.; Xu, H.-Y.; Zhan, L.; Gao, Z.-B.; Yang, J.-L.; Zheng, Y.-M. (–)-Naringenin 4',7-dimethyl Ether Isolated from *Nardostachys jatamansi* Relieves Pain through Inhibition of Multiple Channels. *Molecules* **2022**, *27*, 1735. <https://doi.org/10.3390/molecules27051735>

Academic Editor: Hinanit Koltai

Received: 28 January 2022

Accepted: 3 March 2022

Published: 7 March 2022

**Publisher's Note:** MDPI stays neutral with regard to jurisdictional claims in published maps and institutional affiliations.



**Copyright:** © 2022 by the authors. Licensee MDPI, Basel, Switzerland. This article is an open access article distributed under the terms and conditions of the Creative Commons Attribution (CC BY) license (<https://creativecommons.org/licenses/by/4.0/>).

**Abstract:** (–)-Naringenin 4',7-dimethyl ether ((–)-NRG-DM) was isolated for the first time by our lab from *Nardostachys jatamansi* DC, a traditional medicinal plant frequently used to attenuate pain in Asia. As a natural derivative of analgesic, the current study was designed to test the potential analgesic activity of (–)-NRG-DM and its implicated mechanism. The analgesic activity of (–)-NRG-DM was assessed in a formalin-induced mouse inflammatory pain model and mustard oil-induced mouse colorectal pain model, in which the mice were intraperitoneally administrated with vehicle or (–)-NRG-DM (30 or 50 mg/kg) ( $n = 10$  for each group). Our data showed that (–)-NRG-DM can dose dependently (30~50 mg/kg) relieve the pain behaviors. Notably, (–)-NRG-DM did not affect motor coordination in mice evaluated by the rotarod test, in which the animals were intraperitoneally injected with vehicle or (–)-NRG-DM (100, 200, or 400 mg/kg) ( $n = 10$  for each group). In acutely isolated mouse dorsal root ganglion neurons, (–)-NRG-DM (1~30  $\mu\text{M}$ ) potently dampened the stimulated firing, reduced the action potential threshold and amplitude. In addition, the neuronal delayed rectifier potassium currents ( $I_K$ ) and voltage-gated sodium currents ( $I_{Na}$ ) were significantly suppressed. Consistently, (–)-NRG-DM dramatically inhibited heterologously expressed Kv2.1 and Nav1.8 channels which represent the major components of the endogenous  $I_K$  and  $I_{Na}$ . A pharmacokinetic study revealed the plasma concentration of (–)-NRG-DM is around 7  $\mu\text{M}$ , which was higher than the effective concentrations for the  $I_K$  and  $I_{Na}$ . Taken together, our study showed that (–)-NRG-DM is a potential analgesic candidate with inhibition of multiple neuronal channels (mediating  $I_K$  and  $I_{Na}$ ).

**Keywords:** (–)-Naringenin 4',7-dimethyl ether; analgesic candidate; mechanism study; delayed rectifier potassium currents; ion channels

## 1. Introduction

Pain is an unpleasant sensory and emotional experience associated with actual or potential tissue damage [1]. It can be subdivided into somatic pain and visceral pain according to the originating tissue, while it can be categorized into acute and chronic pain based on the ongoing time [2]. As a rising health problem, chronic pain is predicted to affect up to 30% of adults worldwide, and about 70% of patients are refractory to the current

treatments [2,3]. The use of analgesics is one of the main therapies for the treatment of pain. Opioids, currently a mainstay of pain relief drugs, can cause adverse effects such as tolerance, dependence, opioid-use disorders as well as gastrointestinal dysfunction [4–6]. Huge unmet needs remain for patients with chronic inflammatory, musculoskeletal, visceral, and neuropathic pain conditions. There is an urgent need to identify novel non-opioid drugs and investigate the underlying mechanism, thereby benefiting the following structure-activity relationship studies.

The sensing and transmission of pain signals rely critically on the activities of ion channels expressed in afferent pain fibers, especially for the small-diameter dorsal root ganglia (DRG) neurons [7–9]. It is well established that voltage-gated sodium (Nav) and voltage-gated potassium (Kv) channels are responsible for determining the neuronal excitability, and genetic or pharmacological dysfunction of these channels was widely confirmed to cause pain in human and multiple animal models [10,11]. Among the nine reported Nav (Nav1.1~Nav1.9) isoforms, Nav1.7 and Nav1.8 channels are highly distributed in the peripheral nervous system (PNS) [12]. During an action potential, Nav1.7 is poised to help set a voltage threshold for action potential firing, and Nav1.8 contributes substantially to the rising phase of the action potentials in nociceptors during pain sensing [13]. Then, Kv channel-mediated potassium currents terminate the action potential by repolarizing the membrane potential [14,15]. The potassium currents in nociceptive DRG neurons consist of a rapidly inactivating component and a slowly inactivating component, which respectively correspond to the transient outward potassium currents ( $I_A$ ) and delayed rectifier potassium current ( $I_K$ ) [16,17]. The Kv2.1 channels are thought to represent a major component of  $I_K$ , which helps to set the resting membrane potential and shape the action potentials [18–20]. Therefore, modulation of these channels underlies multiple analgesics.

*Nardostachys jatamansi* has been widely used as a folk medicine in China, Nepal, Bhutan, India, and Japan for the treatment of pain, altitude sickness, fever, and wounds [21]. The roots of *N. jatamansi* have neuroprotective, sedative, and analgesic properties, and a variety of active ingredients have been separated from *N. jatamansi*, in which sesquiterpenoids, essential oils, iridoids, triterpenoids, flavonoid, coumarin, and lignin are the main chemical constituents [21–23]. The anti-inflammatory activities of sesquiterpenoids, terpenic coumarin, and phytosterol such as nardosinanonones and narchinol might contribute to the analgesic activities produced by *N. jatamansi* [21,24,25]. Inhibition of the production of NO and inflammatory cytokines (IL-6, PEG2, TNF- $\alpha$  and IFN- $\alpha/\beta$ , etc.) and phosphorylation of MAPK signaling is implicated in the analgesic activity [25–27]. Flavonoids are polyphenolic structures naturally distributed in most plants and consumed daily. They have been widely used for analgesic, anti-inflammatory, and antioxidant effects along with safe preclinical and clinical profiles [28,29]. For example, troxerutin and quercetin act as anti-inflammatory agents that help reduce pain in clinics [30,31]. However, flavonoids with analgesic activities have not been reported from *N. jatamansi*. In the current study, a flavonoid named (–)-naringenin 4',7-dimethyl ether ((–)-NRG-DM) was first isolated from *N. jatamansi* (Figure 1). As a flavonoid originating from a widely used folk medicine for pain relief, we hypothesized that (–)-NRG-DM might have analgesic activity similar to its naringenin prototype which has been reported to alleviate pain in multiple models [32]. To explore the hypothesis, the analgesic activity and the potential side effects of (–)-NRG-DM were examined in a formalin-induced mouse inflammatory pain model, mustard oil-induced mouse colorectal pain model, and mouse rotarod test. The underlying mechanism was studied in acutely isolated mouse small-diameter DRG neurons and heterologous expression cells using a standard whole-cell patch-clamp technique.

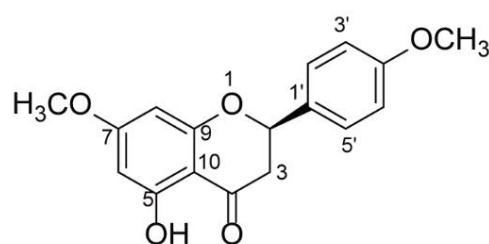


**Figure 1.** The structure of (–)-naringenin 4',7-dimethyl ether ((–)-NRG-DM).

## 2. Results

### 2.1. Structure Elucidation of (–)-NRG-DM

(–)-NRG-DM was obtained as a white needle crystal, which was isolated from *N. jata-mansi* by means of chromatographic methods, including HPLC and silica gel column chromatography. The structural assignments were confirmed by HRESIMS,  $^1\text{H}$ , and  $^{13}\text{C}$  NMR spectra, and compared with the literature data. The molecular formula was confirmed as  $\text{C}_{17}\text{H}_{16}\text{O}_5$  based on its HRESIMS ion at  $m/z$  323.088 5  $[\text{M} + \text{Na}]^+$  (calcd. 323.089 0) and 623.187 9  $[2\text{M} + \text{Na}]^+$  (calcd. 623.188 8). The planar structure of (–)-NRG-DM was confirmed by the NMR data of (–)-NRG-DM, which were those of (+)-naringenin 4',7-dimethyl ether [33,34]. (–)-NRG-DM has only one chiral carbon atom (C-2), and the specific rotation of (–)-NRG-DM was +7.8 (c 0.22 in  $\text{CH}_2\text{Cl}_2$ ), which is contrary to that of sakuranetin [35]. Therefore, the absolute configuration of C-2 of (–)-NRG-DM was determined as R. Thus, the absolute configuration of (–)-NRG-DM was assigned as Figure 1.

### 2.2. Analgesic Effects of (–)-NRG-DM in Formalin-Induced Mouse Inflammatory Pain Model

The formalin test is a classical inflammatory pain model which represents somatic pain. Intraplantar injection of formalin results in a typical two-stage nociceptive behavior, which is characterized by licking and biting of the injected paw. The first phase (0~10 min) mainly reflects nociceptive pain, while the second phase (11~60 min) represents the inflammatory responses [36]. In our study, we tested the effects of (–)-NRG-DM on formalin-induced inflammatory pain in mice. (–)-NRG-DM at 30 mg/kg and 50 mg/kg body weight were individually intraperitoneally administrated 30 min before injection of 1% formalin solution. Consequently, (–)-NRG-DM significantly attenuated painful behaviors in a dose-dependent manner during phase I and phase II (Figure 2). At the dose of 50 mg/kg, (–)-NRG-DM significantly attenuated painful behaviors, including the licking time and overall pain score in both phases in formalin-injected mice. While at the dose of 30 mg/kg, (–)-NRG-DM shortened the licking time and pain score of the two behavioral stages, but only had a significant influence in phase I.

To exclude possible non-specific muscle relaxant or sedative effects, the effects of (–)-NRG-DM on motor performance were evaluated in the rotarod test. (–)-NRG-DM was well tolerated in the rotarod test, with no significant effects on the ability to remain on the rotating rod after intraperitoneal administration of (–)-NRG-DM at 100 mg/kg, 200 mg/kg, or even 400 mg/kg (Table 1). Together, these data showed that (–)-NRG-DM is a well-tolerated natural analgesic compound and can dose-dependently suppress somatic pain in vivo.

### 2.3. Analgesic Effects of (–)-NRG-DM in Mustard Oil-Induced Mouse Colorectal Pain Model

The dose-dependent relief of somatic pain in the formalin model prompted us to ask whether it could attenuate the visceral pain. Thereby, we constructed the mustard oil-induced mouse colorectal pain model as previously described [37]. After intracolonic application of 50  $\mu\text{L}$  0.75% mustard oil, the mice exhibited pain-related behavior (e.g., licking, stretching, squashing, or retraction of the abdomen) in the next 30 min observation period (Figure 3A). As those observed in intraplantar formalin-induced pain, (–)-NRG-DM dose dependently relieved intracolonic mustard oil-caused writhing (Figure 3A). After intraperitoneal application of 30 mg/kg and 50 mg/kg (–)-NRG-DM, the writhing number

reduced by approximately 60% and 80%, respectively (Figure 3B). Our data showed that (–)-NRG-DM could attenuate visceral pain either.

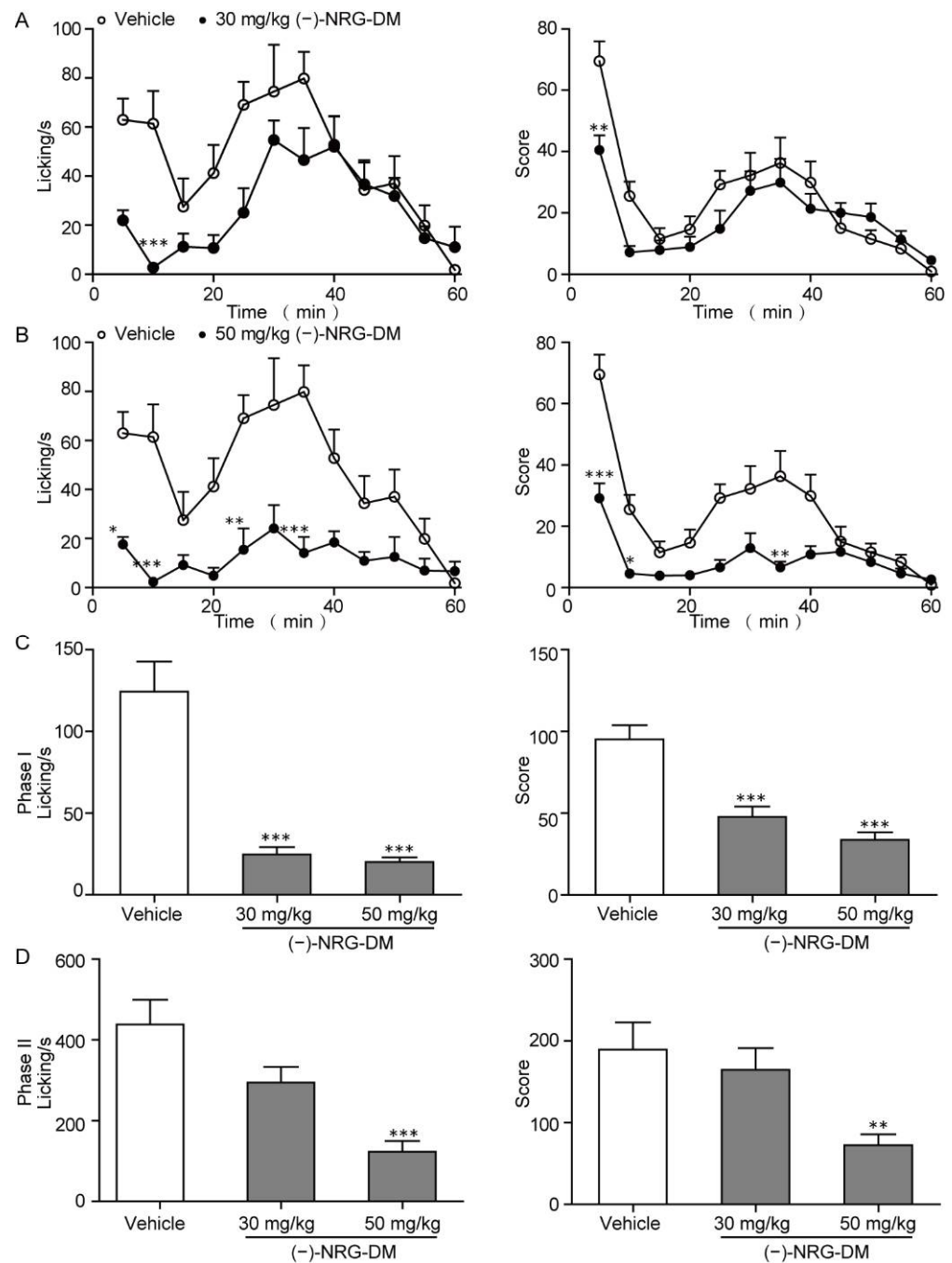


**Figure 2.** Analgesic effects of (–)-NRG-DM in the formalin-induced mouse inflammatory pain model. (A) 30 mg/kg compound (–)-NRG-DM attenuated the biphasic pain responses, including both licking time (left) and score (right) throughout the 60 min trial. (B) 50 mg/kg (–)-NRG-DM attenuated the biphasic pain responses, including both licking time (left) and score (right) throughout the 60 min trial. Bar graph showing the effects of vehicle (white), 30 mg/kg and 50 mg/kg compound (–)-NRG-DM (grey) on the pain behaviors during phase I (C) and phase II (D) in the formalin-induced mouse inflammatory pain model. In all groups,  $n = 10$  animals. Statistical significance: \*  $p \leq 0.05$ , \*\*  $p \leq 0.01$ , \*\*\*  $p \leq 0.001$ .

**Table 1.** Effects of (–)-NRG-DM on motor impairment in the rotarod test in ICR mice.

Compound	Dosage (mg/kg)	Time of Test (h)	Fall $n_{\text{Fall}}/n_{\text{Test}}$	Motor Impairment (%)
Vehicle	-	0.5	0/10	0
		1	0/10	0
		0.5	0/10	0
		1	0/10	0
(–)-NRG-DM	200	0.5	1/10	10
		1	0/10	0
		0.5	0/10	0
		1	0/10	0
(–)-NRG-DM	400	0.5	0/10	0
		1	0/10	0

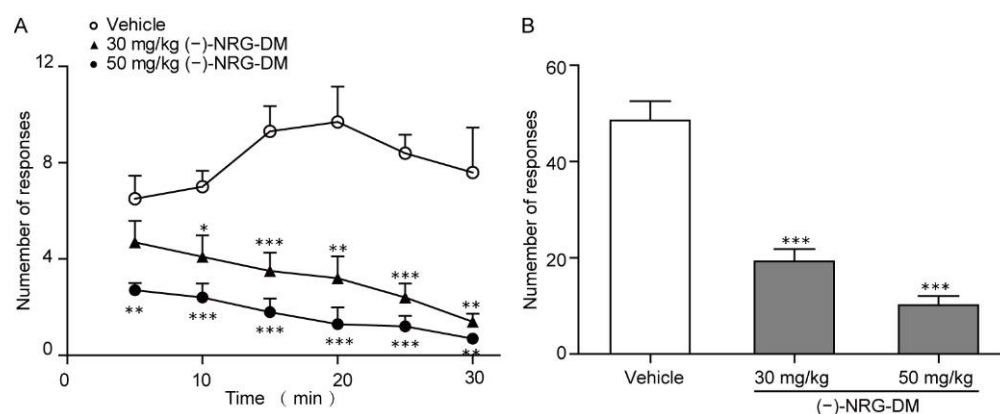


**Figure 3.** Analgesic effects of (–)-NRG-DM in the mustard oil-induced mouse colorectal pain model. (A) 30 mg/kg and 50 mg/kg (–)-NRG-DM attenuated the acute pain-related behaviors throughout the 30 min trial. (B) Bar graph showing the effects of vehicle (white), 30 mg/kg and 50 mg/kg (–)-NRG-DM (grey) on the writhing number caused by pain during a 30 min period in the mustard oil-induced mouse colorectal pain model. In all groups,  $n = 10$  animals. Statistical significance: \*  $p \leq 0.05$ , \*\*  $p \leq 0.01$ , \*\*\*  $p \leq 0.001$ .

#### 2.4. Inhibitory Effects of (–)-NRG-DM on Action Potential Firing in Mouse DRG Neurons

To investigate the underlying mechanism of (–)-NRG-DM-mediated analgesic activity, whole-cell current-clamp technology was applied to examine the effects of (–)-NRG-DM on the action potential firing in acutely isolated mouse small-diameter DRG neurons. The action potentials were evoked by a current injection of 200 pA for a 500 ms period. The threshold was defined by the first amplitude at which an action potential with a membrane potential larger than 0 mV was produced, and the amplitude was defined as the peak relative to the resting membrane potential [38]. Consistent with its analgesic activities in vivo, (–)-NRG-DM dose-dependently inhibited the firing frequency of the DRG neurons (Figure 4A,B). The amplitudes were reduced from  $98.00 \pm 6.19$  mV to  $95.00 \pm 5.65$  mV,  $93.40 \pm 8.27$  mV,  $86.80 \pm 9.75$  mV, and  $74.40 \pm 7.08$  mV after perfusion of 1  $\mu\text{M}$ , 3  $\mu\text{M}$ , 10  $\mu\text{M}$ , and 30  $\mu\text{M}$  (–)-NRG-DM, respectively (Figure 4C,  $n = 5$ ). Current threshold, the injection current required to elicit a single all-or-none action potential, was determined by applying 500 ms depolarizing currents of increasing magnitude. Surprisingly, the threshold of action potential firing was gradually reduced as the concentration of (–)-NRG-DM increased (Figure 4D, E,  $n = 5$ ). The inhibitory effects of (–)-NRG-DM on the firing frequency and the amplitudes of action potentials were partially reversible after washout. These data indicated that (–)-NRG-DM can dampen action potential discharges in nociceptive DRG neurons.

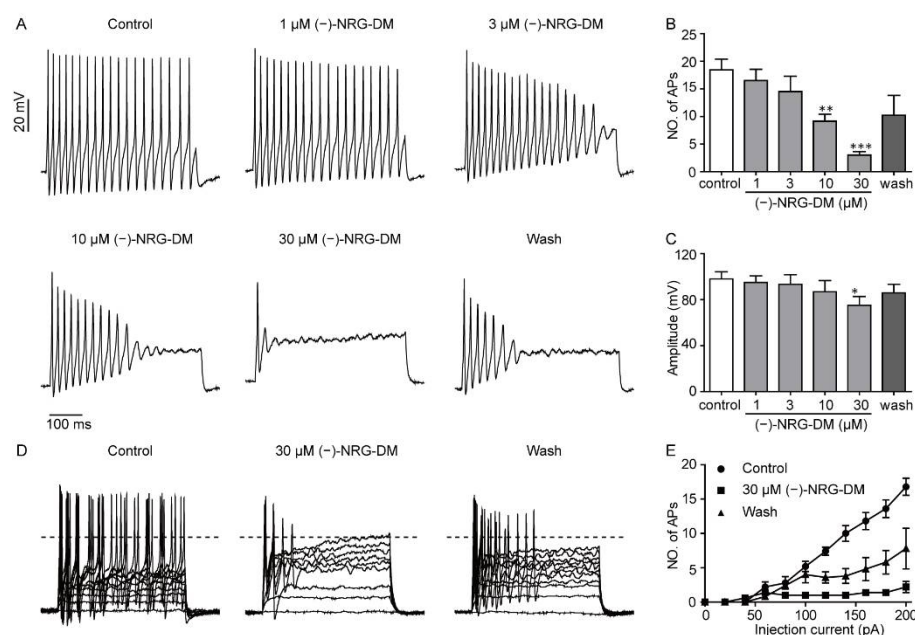


**Figure 4.** (–)-NRG-DM inhibited the neuronal excitability of acutely isolated mouse dorsal root ganglion neurons. (A) Representative traces of action potentials following 200 pA current injection with or without (–)-NRG-DM at indicated concentrations in DRG neurons. Bar graph showing the effects of (–)-NRG-DM on the firing frequency (B), amplitudes of the first action potential (C) before (control, white) and after the application of (–)-NRG-DM (grey) at indicated concentrations ( $n \geq 5$ ). (D) Responses of representative DRG neurons with or without 30  $\mu\text{M}$  (–)-NRG-DM to 500 ms depolarization current steps for the generation of all-or-none action potential. (E) The averaged number of action potentials of DRG neurons before and after application of 30  $\mu\text{M}$  (–)-NRG-DM ( $n = 5$ ). Statistical significance: \*  $p \leq 0.05$ , \*\*  $p \leq 0.01$ , \*\*\*  $p \leq 0.001$ .

### 2.5. Inhibitory Effects of (–)-NRG-DM on Neuronal Potassium Currents

(–)-NRG-DM treatment caused a significant decrease in the current threshold for DRG neurons indicating that the compound may inhibit the potassium currents. The currents in mouse DRG neurons can be separated into  $I_A$  and  $I_K$ . They could be distinguished by applying voltage steps from a holding potential of  $-50$  mV, at which  $I_A$  was almost completely inactivated, while  $I_K$  remained unchanged. Thereby,  $I_A$  could be separated by subtracting  $I_K$  from the total potassium currents. According to these electrophysiological characteristics, the effects of (–)-NRG-DM on potassium currents were examined (Figure 5A). We found that (–)-NRG-DM inhibited potassium currents in a dose-dependent manner, and the  $IC_{50}$  values were  $5.10 \pm 0.04$   $\mu\text{M}$  and  $119.90 \pm 0.03$   $\mu\text{M}$  for  $I_K$  and  $I_A$ , respectively (Figure 5B,  $n = 5$ ). The data indicated that (–)-NRG-DM is an inhibitor of  $K_v$  channels in DRG neurons. Additionally, the effects of (–)-NRG-DM on the kinetics of the  $K_v$  channels were further characterized. The  $K_v$  currents were elicited by multiple 1500 ms depolarization pulses ranging from  $-80$  mV to  $+90$  mV in 10 mV increments from a holding potential of  $-80$  mV. Congruently, the amplitudes of elicited potassium currents were potently reduced by (–)-NRG-DM at 10  $\mu\text{M}$ , a concentration around  $IC_{50}$  of (–)-NRG-DM on  $I_K$  currents (Figure 5C). The activation curves of  $K_v$  channels before and after the perfusion of 10  $\mu\text{M}$  (–)-NRG-DM were fitted with the Boltzmann equation, the data showed that (–)-NRG-DM does not affect the activation of the potassium currents (Figure 5D). The values of  $V_{1/2}$  in the absence and presence of 10  $\mu\text{M}$  (–)-NRG-DM were  $-6.43 \pm 1.21$  mV and  $-8.08 \pm 2.02$  mV, respectively (Figure 5D). These data showed that (–)-NRG-DM is an inhibitor of native potassium currents in DRG neurons.

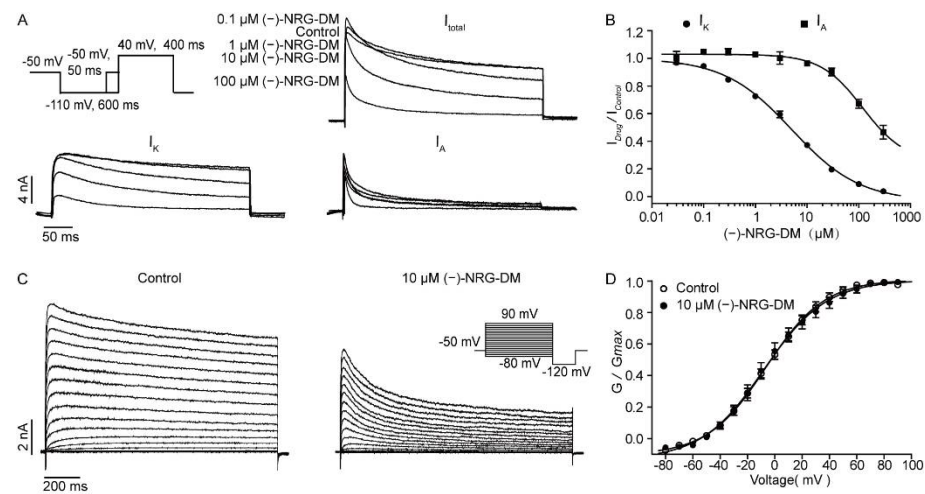


**Figure 5.** Inhibitory effects of (-)-NRG-DM on the potassium currents of DRG neurons in mice. (A) Typical traces of the transient outward potassium currents  $I_A$  and the delayed rectifier potassium currents  $I_K$  in the presence of (-)-NRG-DM at indicated concentrations. (B) The dose–response curve of (-)-NRG-DM on  $I_K$  and  $I_A$  currents. The  $IC_{50}$  values were  $5.10 \pm 0.04 \mu$ M and  $119.90 \pm 0.03 \mu$ M, respectively ( $n = 5$ ). (C) Representative activation current traces of Kv channels before and after 10  $\mu$ M (-)-NRG-DM. (D) Activation curves of Kv currents before and after 10  $\mu$ M of (-)-NRG-DM ( $n = 6$ ).

### 2.6. Inhibition of (-)-NRG-DM on Neuronal Sodium Currents

A reduction in amplitudes of action potentials manifested that (-)-NRG-DM may inhibit native sodium currents, which are mainly involved in the rising phase of an action potential [39]. To record native sodium currents in acutely isolated DRG neurons, a 50 ms test pulse depolarized to  $-20$  mV from a holding potential of  $-90$  mV was applied. As illustrated in Figure 6A, the amplitudes of peak currents and persistent currents dose-dependently declined as the concentration of (-)-NRG-DM increased. The  $IC_{50}$  value of (-)-NRG-DM on native Nav currents was  $34.78 \pm 0.14 \mu$ M (Figure 6C,  $n = 5$ ). To understand how (-)-NRG-DM inhibited Nav channels, the effects of 30  $\mu$ M compound (-)-NRG-DM on Nav channel kinetics were further characterized. The activation currents were elicited by applying step pulses ranging from  $-60$  mV to  $+15$  mV in 5 mV increments for a 50 ms period from a holding potential of  $-90$  mV (Figure 6D). The activation curves showed that the half-activation voltage did not change significantly after the perfusion of 30  $\mu$ M (-)-NRG-DM, and the  $V_{1/2}$  values were  $-15.34 \pm 0.58$  mV and  $-15.23 \pm 0.56$  mV, respectively (Figure 6E). The influence of 30  $\mu$ M (-)-NRG-DM on steady-state inactivation was assessed by 500 ms conditioning pulses ramping from  $-120$  mV to 0 mV in 10 mV increments, followed by a 20 ms test pulse at  $-20$  mV (Figure 6F). In contrast to the lack of effect on the Nav channel activation, (-)-NRG-DM caused a depolarization shift of the steady-state inactivation. The  $V_{1/2}$  value was shifted from  $-65.72 \pm 1.74$  mV to  $-55.34 \pm 2.14$  mV by 30  $\mu$ M (-)-NRG-DM (Figure 6G). These data showed that (-)-NRG-DM is an inhibitor of native sodium channels in small-diameter DRG neurons.

The sodium currents in small-diameter DRG neurons could be further subdivided into TTX-sensitive (TTX-S) and TTX-resistant (TTX-R) currents, which contribute to setting the firing threshold and the rising phase of an action potential [40]. To isolate TTX-R currents, whole-cell sodium currents were measured in the presence of 300 nM TTX. Similar to its effect on total sodium currents, (-)-NRG-DM did not affect the activation either (Figure 6I). The values of  $V_{1/2}$  in the absence and presence of 30  $\mu$ M (-)-NRG-DM were  $-16.82 \pm 0.72$  mV and  $-20.14 \pm 0.87$  mV, respectively. Notably, (-)-NRG-DM caused a hyperpolarizing shift in steady-state inactivation. The value of  $V_{1/2}$  shifted from  $-39.43 \pm 0.66$  mV to  $-49.99 \pm 0.67$  mV by 30  $\mu$ M (-)-NRG-DM (Figure 6K). These data

indicated that (–)-NRG-DM is an inhibitor of sodium currents and preferentially affects channel inactivation.

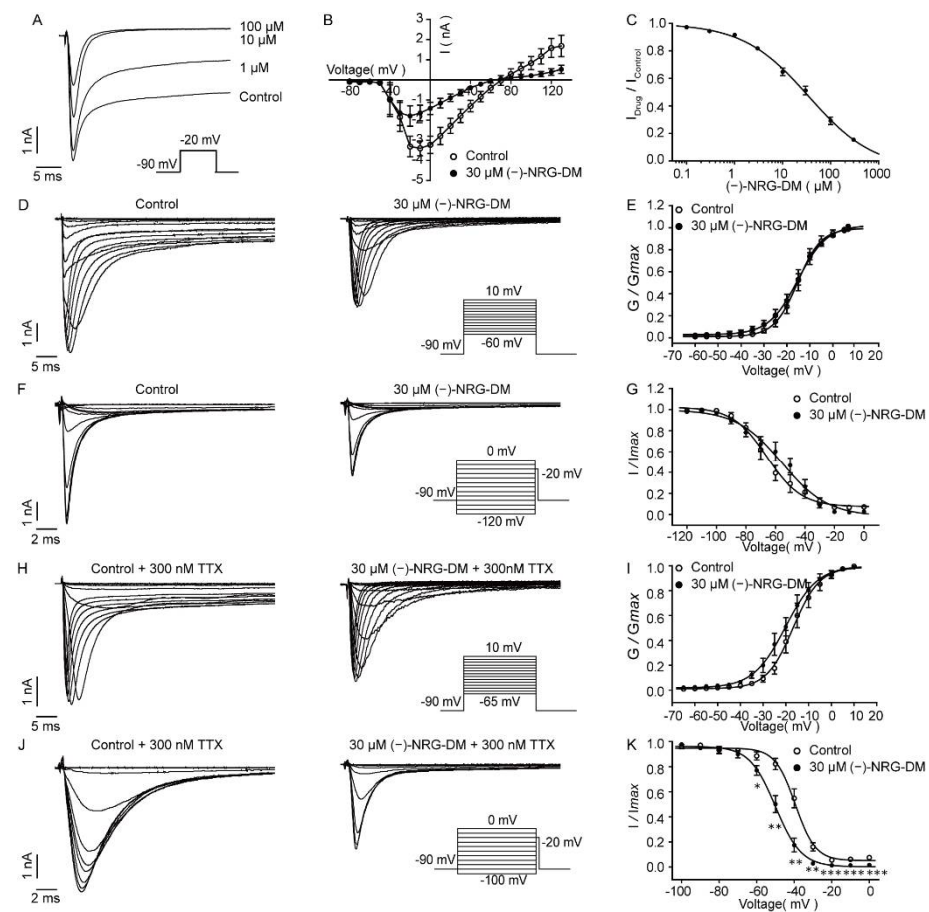


**Figure 6.** Characterization of (–)-NRG-DM inhibition on Nav currents of DRG neurons in mice. (A) Representative traces of Nav currents in the absence or presence of (–)-NRG-DM at indicated concentrations. (B) Current–voltage relationship of Nav currents with or without 30  $\mu\text{M}$  (–)-NRG-DM ( $n = 8$ ). (C) The dose–response curve of (–)-NRG-DM on native Nav currents. The  $\text{IC}_{50}$  value was  $34.78 \pm 0.14 \mu\text{M}$  ( $n = 5$ ). Typical activation current traces (D) and steady-state activation curves (E) of total Nav currents before and after application of 30  $\mu\text{M}$  (–)-NRG-DM ( $n = 6$ ). Representative inactivation traces (F) and steady-state inactivation curves (G) of total Nav currents before and after perfusion of 30  $\mu\text{M}$  (–)-NRG-DM ( $n = 6$ ). Typical activation current traces (H) and steady-state activation curves (J) of TTX-R currents before and after perfusion of 30  $\mu\text{M}$  (–)-NRG-DM ( $n = 7$ ). Representative inactivation traces (I) and steady-state inactivation curves (K) of TTX-R currents before and after perfusion of 30  $\mu\text{M}$  (–)-NRG-DM ( $n = 7$ ). Statistical significance: \*  $p \leq 0.05$ , \*\*  $p \leq 0.01$ , \*\*\*  $p \leq 0.001$ .

### 2.7. Inhibitory Effects of (–)-NRG-DM on Heterologously Expressed Kv2.1 Channel

Kv2.1 represents a major component of  $\text{I}_\text{K}$  currents in neurons and plays an important role in the formation of functional Kv channels [18,41]. The potent inhibitory effects of (–)-NRG-DM on native potassium currents in DRG neurons prompted us to investigate whether the natural analgesic compound affects Kv2.1 channels transiently expressed in CHO cells. Congruently, (–)-NRG-DM dose-dependently inhibited Kv2.1 channels with an  $\text{IC}_{50}$  value of  $21.17 \pm 0.11 \mu\text{M}$  (Figure 7A,  $n = 5$ ). The typical Kv2.1 current was elicited by applying a 40 mV depolarization stimulus before and after application of (–)-NRG-DM at 20  $\mu\text{M}$ , a concentration around the  $\text{IC}_{50}$  of Kv2.1 channels, as illustrated in Figure 7B. The effects of 20  $\mu\text{M}$  (–)-NRG-DM on the activation of Kv2.1 channels were further evaluated. The activation currents of Kv2.1 were elicited by applying multiple pulses ranging from



–80 mV to +110 mV in 10 mV increments for a 1500 ms period from a holding potential of –50 mV (Figure 7D). Surprisingly, the value of  $V_{1/2}$  shifted from  $22.30 \pm 1.12$  mV in the control condition to  $35.88 \pm 1.88$  mV in the presence of 20  $\mu$ M (–)-NRG-DM (Figure 7E). These data showed that (–)-NRG-DM is an inhibitor of the Kv2.1 channel and dampens channel activation.

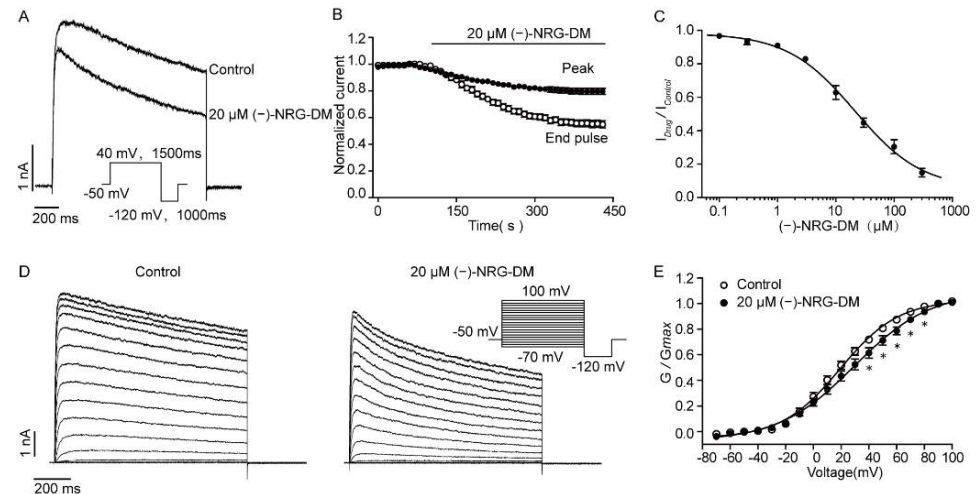


**Figure 7.** Inhibitory effects of (–)-NRG-DM on Kv2.1 channels heterologously expressed in CHO cells. (A) Representative Kv2.1 current traces in the absence and presence of 20  $\mu$ M (–)-NRG-DM (Inset) The recording protocol. (B) Time course of peak and end-pulse currents of Kv2.1 channels before and after perfusion of 20  $\mu$ M (–)-NRG-DM. (C) The dose–response curve of (–)-NRG-DM on Kv2.1 channel. The  $IC_{50}$  value was  $21.17 \pm 0.11$   $\mu$ M ( $n = 5$ ). (D) Representative activation current traces of Kv2.1 channels in absence and presence of 20  $\mu$ M (–)-NRG-DM (Inset) The recording protocol. (E) Activation curves of Kv2.1 channels with or without 20  $\mu$ M (–)-NRG-DM ( $n = 5$ ). Statistical significance: \*  $p \leq 0.05$ .

## 2.8. (–)-NRG-DM Inhibits Nav Channels

The dose-dependent suppression of the sodium currents by (–)-NRG-DM indicated that it should inhibit the Nav channels. As Nav1.7 and Nav1.8 are mainly distributed in the PNS and have been demonstrated to play an important role in pain sensing, we detected the effects of (–)-NRG-DM on Nav1.7 and Nav1.8 channels stably expressed in HEK293 cells. As shown in Figure 8A, we found that 30  $\mu$ M (–)-NRG-DM, a concentration around the  $IC_{50}$  of native Nav currents in DRG neurons, can potently inhibit Nav1.7 and Nav1.8 currents. The values of  $I_{Drug}/I_{Control}$  were  $0.61 \pm 0.05$  and  $0.56 \pm 0.03$ , respectively (Figure 8B). There is no significant difference in the inhibitory efficacy between Nav1.7 and Nav1.8 channels; the data showed that (–)-NRG-DM is a non-selective Nav channel inhibitor (Figure 8B). To understand how (–)-NRG-DM inhibits Nav1.8 channels, we assessed its impacts on the voltage dependence of steady-state activation and inactivation. The Nav1.8 currents were elicited by applying step pulses ranging from –65 mV to +30 mV for 200 ms in 5 mV increments at a stimulus frequency of 0.5 Hz (Figure 8C). Activation curves showed that the  $V_{1/2}$  did not change significantly before and after the perfusion of 30  $\mu$ M (–)-NRG-DM, which was  $-7.10 \pm 1.10$  mV and  $-10.31 \pm 1.17$  mV, respectively (Figure 8D). The influence of (–)-NRG-DM on steady-state inactivation was evaluated by applying a 500 ms conditioning pulse ramping from –110 mV to 10 mV in 10 mV increments, followed by a 20 ms test pulse at –20 mV (Figure 8E). The values of  $V_{1/2}$  were  $-48.58 \pm 0.67$  mV and  $-53.37 \pm 0.70$  mV before and after the application of 30  $\mu$ M (–)-NRG-DM (Figure 8F). Similarly, no significant difference was observed. These data showed that (–)-NRG-DM is a nonselective inhibitor of Nav channels.

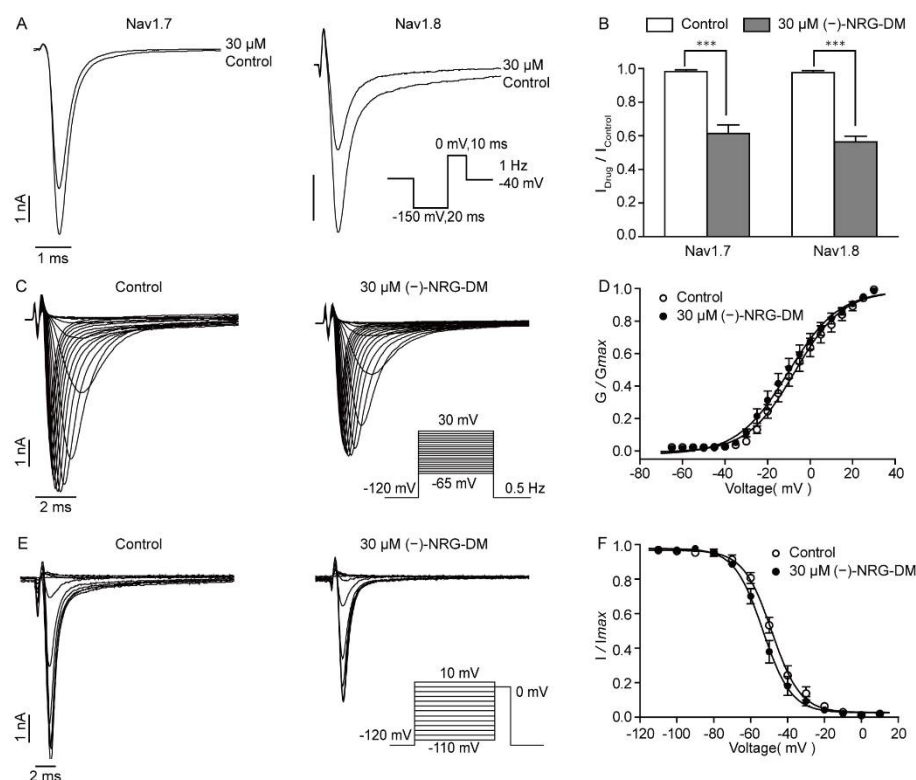


**Figure 8.** Inhibitory effect of (–)-NRG-DM on Nav currents. (A) Representative Nav1.7 and Nav1.8 current traces in the absence and presence of 30  $\mu\text{M}$  (–)-NRG-DM recorded with the depicted protocol. (B) Summarized data showing the suppression effect of (–)-NRG-DM (30  $\mu\text{M}$ ) on Nav1.7 and Nav1.8 channels ( $n = 5$ ). (C) Representative Nav1.8 current traces in absence and presence of 30  $\mu\text{M}$  (–)-NRG-DM recorded with the protocol shown inset. (D) Activation curves obtained in the absence and presence of 30  $\mu\text{M}$  (–)-NRG-DM ( $n = 13$ ). (E) Representative activation current traces of Nav1.8 currents before and after 30  $\mu\text{M}$  (–)-NRG-DM. (F) Steady-state inactivation curve of Nav1.8 currents before and after 30  $\mu\text{M}$  (–)-NRG-DM ( $n = 13$ ). Statistical significance: \*\*\*  $p \leq 0.001$ .

### 3. Discussion

In the present study, a naringenin derivative named (–)-NRG-DM was first isolated from *N. jatamansi* (Figure 1). Intraperitoneal administration of (–)-NRG-DM dose-dependently attenuated pain in a formalin-induced mouse inflammatory pain model and mustard oil-induced mouse colorectal pain model, which, respectively, corresponded to somatic pain and visceral pain (Figures 2 and 3). Notably, (–)-NRG-DM was well tolerated as no significant neurotoxicity was observed at doses of 100 mg/kg, 200 mg/kg, and even 400 mg/kg in the rotarod test (Table 1). All animals displayed no sign of toxicity during the rotarod test (0.5 and 1 h) and 24 h after the drug administration. The data showed that (–)-NRG-DM is an analgesic compound with a wide margin of safety. Combining the data obtained from the acutely isolated mouse small-diameter DRG neurons, heterologous expression system, and pharmacokinetic study, we furtherly elucidated that inhibition of neuronal channels mediating  $I_K$  and  $I_{Na}$  currents is implicated in the (–)-NRG-DM-produced analgesic activity.

The current study showed that the analgesic (–)-NRG-DM directly dampens neuron excitability in acutely isolated mouse small-diameter DRG neurons with a reduced threshold and amplitude of action potential firing (Figure 4A). Intriguingly, the suppression of firing frequency is tightly accompanied by a depolarized firing threshold (Figure 4A,D). The significant reduction in the number of action potentials started after 10  $\mu\text{M}$  (–)-NRG-DM was applied, at which the significant difference in the firing threshold occurred (Figure 4D,E). The data suggested that (–)-NRG-DM may cause suppression through a mechanism similar to neuronal desensitization. The feature is involved in capsaicin,

a TRPV1 channel agonist, and an 8% capsaicin patch (Qutenza) has been approved for the treatment of chronic pain in clinics [42]. Analgesic activities produced by a direct desensitization of nociceptive neurons might reduce side effects including gastrointestinal erosions, renal and hepatic insufficiency which are commonly associated with cyclooxygenase inhibitors [43]. As 10  $\mu\text{M}$  (–)-NRG-DM did not affect TRPA1 currents, the neuronal desensitization could not be ascribed to its modulation on the channels (Figure S1). The suppression of neuron activity produced by (–)-NRG-DM is in agreement with the study of (+)-naringenin 4',7-dimethyl ether ((+)-NRG-DM), a naturally occurring naringenin derivative that has been isolated many times from plants, that showed analgesic activity in vivo and that did not influence the production and release of pro-inflammatory factors compared to other naringenin derivatives [44]. Additionally, radioligand binding assay demonstrated that (+)-NRG-DM does not show affinity to endocannabinoid or opioid receptors [22]. Together, our data showed that (–)-NRG-DM causes a direct inhibition of neuron excitability through a mechanism similar to excitatory desensitization in nociceptive neurons.

Voltage-gated potassium currents play a fundamental role in the modulation of resting membrane potential [45]. In the small-diameter DRG neurons, the currents can be divided into two separate components:  $I_A$  and  $I_K$  [46]. Due to the low current density and distribution ratio, the  $I_A$  currents did not seem to play a key role in the excitability of nociceptive neurons. The  $I_K$  currents contribute to the setting of resting membrane potential and appear to be the main contributor to after-hyperpolarization [20,47]. Consistent with the depolarized threshold of action potential firing, (–)-NRG-DM potently inhibited the  $I_K$  but not  $I_A$  currents with  $IC_{50}$  values of  $5.10 \pm 0.04 \mu\text{M}$  and  $119.90 \pm 0.03 \mu\text{M}$ , respectively (Figure 5A,B). Notably, the pharmacokinetic study showed that the plasma concentration of (–)-NRG-DM after 0.5–1.5 h intraperitoneal injection of the compound at 50 mg/kg is around 7  $\mu\text{M}$ , which is higher than the  $IC_{50}$  value of (–)-NRG-DM on  $I_K$  currents (Table 2). The reduction in the  $I_K$  currents in DRG neurons at this concentration was around 58% (Figure 5B). Kv2.1 homotetramers or containing heterotetramers represent the major component of  $I_K$  currents in neurons [18,40]. Consistently, the  $IC_{50}$  value of (–)-NRG-DM on Kv2.1 channels heterologously expressed in CHO cells was  $21.17 \pm 0.11 \mu\text{M}$  (Figure 7A,B). The difference between the  $IC_{50}$  values obtained from DRG neurons and CHO cells may emerge from species differences in primary pharmacology. One might argue that a reduction in the  $I_K$  currents has been found in multiple animal models for studying pain, and lesser  $I_K$  currents are involved in human labor pain [48,49]. The feature might be similar to that found in Nav1.9 channels, in which the gain-of-function mutations caused a loss of pain reception in humans and exhibited a reduced neuronal excitability during the long stimulus due to neuronal desensitization [50]. Thus, our data showed that the inhibition of  $I_K$  mainly contributes to (–)-NRG-DM-produced pain relief and Kv2.1-containing channels involved in the inhibitory activity.

**Table 2.** Mean plasma concentration of (–)-NRG-DM administrated via intraperitoneal route in ICR mice.

Compound	Dosage (mg/kg)	Time of Test (h)	Concentration (ng/mL)	Concentration ( $\mu\text{M/L}$ )
(–)-NRG-DM	50	0.5	$2293.3 \pm 183.4$	$7.64 \pm 0.61$
		1	$2216.0 \pm 1252.0$	$7.39 \pm 4.17$
		1.5	$716.7 \pm 222.5$	$2.39 \pm 0.74$

Data are presented as the mean  $\pm$  SEM.

The reduction in the amplitudes of the action potentials after exposure to (–)-NRG-DM was in accordance with its suppression of sodium currents (Figure 4C). (–)-NRG-DM inhibited Nav currents in DRG neurons in a dose-dependent manner with an  $IC_{50}$  value of  $34.78 \pm 0.14 \mu\text{M}$  (Figure 6C). Nevertheless, a reduction in the  $I_{Na}$  of the DRG neurons was around 28% at the plasma concentration obtained from the pharmacokinetic study (Figure 6C). Nav1.7 and Nav1.8 are analgesic-related Nav subtypes in the PNS,

which separately correspond to the TTX-S and TTX-R currents in small-diameter DRG neurons [46]. The inhibitory ratios of (–)-NRG-DM (30  $\mu$ M) on Nav1.7 and Nav1.8 were  $39 \pm 5\%$  and  $44 \pm 3\%$  respectively, which were very close to those on native sodium currents (Figure 8A,B). As an enantiomer, NRG-DM extracted from peanut stem and leaf promoted sleep by dampening neuronal excitability. In cortical neurons, the inhibitory activity of NRG-DM on Nav channels appeared to be more potent than that on Kv channels [51]. However, in the current study, due to the higher  $IC_{50}$  value, our data showed that inhibition of Nav channels might contribute to (–)-NRG-DM-produced analgesic activity but the effect is secondary to that of Kv channels.

In conclusion, our study showed that (–)-NRG-DM is a promising analgesic drug candidate potentially attenuating somatic and visceral pain in vivo. The analgesic activity could be ascribed to its direct suppression of nociceptive neuron excitability through a desensitization mechanism. Due to the plasma concentration of (–)-NRG-DM being higher than the effective concentrations for the  $I_K$  and  $I_{Na}$ , our study suggested that the inhibition of neuronal channels mediating these currents contributes to the analgesic activity. (–)-NRG-DM may act as a new structural framework for the subsequent development of analgesic drugs.

## 4. Materials and Methods

### 4.1. Chemical Compounds

(–)-NRG-DM, isolated from the roots of *N. jatamansi*, was prepared and certificated by Professor Jun-Li Yang's lab at Lanzhou Institute of Chemical Physics, Chinese Academy of Sciences. The procedure of extraction and isolation of (–)-NRG-DM can be found in the Supporting Information. The compound was dissolved and stored in dimethyl sulfoxide (DMSO) to produce a 20 mM stock solution and then diluted in bath solution to obtain final concentrations. DMSO, at the final concentrations ( $\leq 0.5\%$ ), was well tolerated with no observable toxic effects on cells and neurons. To conduct research on animals, (–)-NRG-DM was dissolved in a mixture of 5% DMSO, 5% Tween 80, and 90% (0.9% NaCl). TTX was purchased from Qinhuangdao Aquaculture Technical Developing Company (Qinhuangdao, China). All other chemicals were purchased from Sigma-Aldrich (St Louis, MO, USA).

### 4.2. Animals

All mice were obtained from the Beijing Vitalriver Laboratory Animal Technology Co., Ltd. (Beijing, China). Mice were housed and assayed under controlled temperature conditions ( $22 \pm 2$  °C) and a 12 h light/dark cycle with free access to food and water. All animal procedures were performed according to the National Institutes of Health Guide for the Care and Use of Laboratory Animals and were strictly followed and approved by the guidelines of the IACUC (Institutional Animal Care and Use Committees). The IACUC checked all protocols and approved this study. The animal experiments were conducted in a blinded manner, i.e., drug administration and behavioral tests were finished by different investigators.

### 4.3. Formalin-Induced Inflammatory Model

Adult male ICR mice weighing  $20 \pm 2$  g were randomly divided into 3 groups ( $n = 10$  for each group) and acclimatized in a transparent observation chamber for at least 30 min before the experiment. Mice were intraperitoneally administrated with vehicle or (–)-NRG-DM (30 or 50 mg/kg) 30 min prior to formalin injection. Then, 1% formalin solution (20  $\mu$ L per site) was subcutaneously injected into the plantar of the left hind paw to induce acute inflammatory pain. Immediately, mice were put back into the observation chambers. Nociception caused by formalin was assessed by scoring painful behaviors and licking time over a period of 60 min. In the present study, the score represented the sum of weighted formalin-induced pain-related behavior: 1 = flinching, 2 = shaking, and 3 = licking or biting of the injected paw. Phases were defined as follows: the peak time of the early nociceptive

response phase (phase I) was 0~10 min, and the late phase (phase II) was 11~60 min after formalin injection.

#### 4.4. Mustard Oil-Induced Mouse Colorectal Pain Model

Male C57BL/6 mice, weighing 23~25 g, were randomly assigned into 3 groups ( $n = 10$  for each group) and placed in a transparent observation chamber for at least 20 min prior to the experiment. Mice were intraperitoneally administrated with vehicle or (–)-NRG-DM (30 or 50 mg/kg) 30 min before the injection of diluted mustard. Subsequently, 50  $\mu$ L of diluted mustard oil solution (0.75% in 70% ethanol) was intracolonicly administrated and the number of pain responses was counted for 30 min. In the present study, postures defined as pain-related behaviors were in agreement with previous descriptions: (1) licking of the abdomen, (2) stretching the abdomen, (3) squashing of lower abdomen against the floor, (4) abdominal wall retractions.

#### 4.5. Rotarod Test

To determine the neurotoxicity effects of (–)-NRG-DM, the standardized rotarod test was conducted in male ICR mice weighted  $20 \pm 2$  g. The mice were divided at random into 4 groups ( $n = 10$  for each group). The mice were placed on a rotarod appliance (YLS-4C, Bio-will, Shanghai, China) with a rod of 3 cm diameter, rotating at a constant speed of 6 rpm. The day before the compound test, all mice were pre-trained and only the animals able to remain on the rod for at least 1 min every time in three consecutive trials (3 min) were retained. During the test, the mice were measured in the rotarod test 0.5 h and 1 h after intraperitoneal administration of (–)-NRG-DM. The animals unable to remain on the rod for 3 consecutive periods were considered motor coordination impaired.

#### 4.6. Pharmacokinetic Study

The pharmacokinetic study was performed in male ICR mice weighted  $20 \pm 2$  g. The mice were fasted for 12 h before intraperitoneal administration of (–)-NRG-DM at 50 mg/kg. Blood samples (0.5 mL) were collected at 0.5, 1, and 1.5 h from the abdominal aorta into the heparinized tubes after drug administration. The plasma was separated by centrifugation (11,000 rpm for 5 min) and then stored at  $-80$  °C until analyzed. Plasma samples (20  $\mu$ L) were treated with the addition of the internal standard solution (20  $\mu$ L) and acetonitrile (300  $\mu$ L), then vortexed for 15 min (1000 rpm, RT), and centrifuged of 15 min (3700 rpm, 4 °C). The supernatants were collected for analysis using LC–MS/MS. The data were processed using Analyst software version 1.6.3 (Sciex, ON, Canada).

#### 4.7. Preparation of Dorsal Root Ganglion Neurons

Dorsal root ganglia (DRG) were dissected from male C57BL/6 mice aged 4~6 weeks. The ganglia were first cut into small pieces and then digested at 37 °C for 20 min in DMEM containing 1 mg/mL collagenase type I and 0.25 mg/mL trypsin (Sigma-Aldrich). Subsequently, the digested small fragments were terminated and resuspended with DMEM/F12 growth medium (Gibco) supplemented with 10% fetal bovine serum (FBS) (Gibco). Finally, the dissociated DRG neurons were seeded onto 24-well plates with poly-L-lysine-coated coverslips and placed in a 37 °C, 5% CO<sub>2</sub> incubator for at least 1 h before electrophysiological experiments.

#### 4.8. Cell Culture and Transfection

Human embryonic kidney 293 (HEK293) cells stably expressing human Nav1.7 and Nav1.8 channels were grown in a high-glucose DMEM medium (Gibco) containing 10% FBS (Gibco). The media were respectively supplemented with 50 mg/mL and 100 mg/mL hygromycin B (Invitrogen, Carlsbad, CA, USA). The cDNA encoding human Kv2.1 channels was synthesized by Sangon Biotech Co., Ltd. (Shanghai, China) based on the GenBank (Kv2.1 Gene ID: 25736) and was subcloned into the pcDNA3.1(+) vector. Chinese hamster ovary (CHO) cells were cultured in DMEM/F12 medium (Gibco) supplemented with

10% FBS. To transiently express the Kv2.1 channels for electrophysiological studies, the constructs encoding the EGFP and the Kv2.1 were co-transfected into the CHO cells with Lipofectamine 2000 reagent (Invitrogen) referring to the manufacturer's instructions. The transfected cells were seeded onto poly-L-lysine-coated glass coverslips before they were used for the electrophysiological study. All cells were grown under standard tissue culture conditions (5% CO<sub>2</sub>, 37 °C).

#### 4.9. Electrophysiological Recordings

A standard whole-cell voltage-clamp technique was used to record membrane currents from the heterologous expression cells and the acutely isolated DRG neurons. A standard whole-cell current-clamp mode was applied to record the action potential (AP) firing in DRG neurons. Pipettes were pulled from borosilicate glass capillaries and the resistances of pipettes were 3~5 MΩ when they were filled with the intracellular solution and placed in the bath. For the recording of potassium currents from the transfected CHO cells, the pipette or intracellular solution contained (in mM): 145 KCl, 10 HEPES, 1 MgCl<sub>2</sub>, 5 EGTA, 1 CaCl<sub>2</sub>, and 10 HEPES (pH 7.2 adjusted by KOH); bath or extracellular solution contained (in mM): 140 NaCl, 5 KCl, 2 CaCl<sub>2</sub>, 1 MgCl<sub>2</sub>, 10 glucose, and 10 HEPES (pH 7.4 adjusted by NaOH). For the recording of sodium currents from the stable cell lines, the pipette or intracellular solution contained (in mM): 140 CsF, 10 NaCl, 20 glucose, 1.1 EGTA, and 10 HEPES (pH 7.3 adjusted with CsOH); bath or extracellular solution contained (in mM): 140 NaCl, 3 KCl, 1 CaCl<sub>2</sub>, 1 MgCl<sub>2</sub>·6H<sub>2</sub>O, 20 glucose, and 10 HEPES (pH 7.3 adjusted by NaOH). For recordings of the action potential firing properties and potassium currents in DRG neurons, the pipette or intracellular solution contained (in mM): 140 KCl, 1 CaCl<sub>2</sub>, 1 MgCl<sub>2</sub>, 10 EGTA, and 10 HEPES (pH 7.2 adjusted with KOH); the extracellular solution contained (in mM): 140 NaCl, 5 KCl, 1 CaCl<sub>2</sub>, 1.25 MgCl<sub>2</sub>, 10 glucose, and 10 HEPES (pH 7.4 adjusted with NaOH). For the recording of neuronal sodium currents from DRG neurons, the pipette or intracellular solution contained (in mM): 120 CsCl, 10 NaCl, 10 TEA-Cl, 1 CaCl<sub>2</sub>, 1 MgCl<sub>2</sub>, 10 EGTA, and 10 HEPES (pH 7.2 adjusted with CsOH); bath or extracellular solution contained (in mM): 120 NaCl, 5 KCl, 1 CaCl<sub>2</sub>, 1.25 MgCl<sub>2</sub>, 20 TEA-Cl, 10 glucose, and 10 HEPES (pH 7.4 adjusted by NaOH). During the recordings, a BPS perfusion system (ALA Scientific Instruments, Westbury, NY, USA) was used to continuously perfuse bath solutions. Data acquisition was performed at room temperature with the Axopatch-200B amplifier (Axon Instruments, Burlingame, CA, USA), and the signals were filtered at 2 kHz and digitized with a Digidata 1440 A interface (Axon Instruments) at 50 kHz.

#### 4.10. Statistics

Patch-clamp data were processed using Clampfit 10.6 (Molecular Device, Sunnyvale, CA, USA) and then analyzed in GraphPad Prism 5 (GraphPad Software, San Diego, CA, USA). Voltage-dependent activation curves were fitted to the Boltzmann equation:  $G = G_{\min} + (G_{\max} - G_{\min}) / [1 + \exp(V - V_{1/2}) / S]$ , where  $G_{\max}$  is the maximum conductance,  $G_{\min}$  is the minimum conductance,  $V_{1/2}$  is the voltage to reach 50% of the maximum conductance, and  $S$  is the slope factor. Steady-state inactivation curves were constructed by plotting the normalized peak currents during the test pulses as a function of the prepulse potentials. The data were fitted to the Boltzmann equation:  $I / I_{\max} = 1 / \{1 + \exp[(V - V_{1/2}) / K_i]\}$ , where  $I$  is the amplitude of peak currents at each voltage,  $I_{\max}$  is the maximal value of peak currents,  $V$  and  $V_{1/2}$  are the prepulse potential and the half-maximal potential for inactivation, respectively, and  $K_i$  is the inactivation slope factor. Dose-response curves were fitted with the Hill equation:  $Y = \text{Bottom} + (\text{Top} - \text{Bottom}) / [1 + 10^{(\log IC_{50} - X) \times k}]$ , where Bottom and Top are the minimum and maximum inhibition, respectively;  $X$  is the log of the concentration;  $Y$  is the value of  $I_{\text{Drug}} / I_{\text{Control}}$ ;  $IC_{50}$  is the drug concentration producing a half-maximum response,  $k$  is the Hill Slope. The data are shown as the mean  $\pm$  SEM, and the significance was estimated using paired two-tailed Student's  $t$ -test unless otherwise stated. Statistical significance: \*  $p \leq 0.05$ , \*\*  $p \leq 0.01$ , \*\*\*  $p \leq 0.001$ .

**Supplementary Materials:** The following supporting information is available online, Figure S1: The effects of (–)-NRG-DM on TRPA1 channels; Figure S2: HRESIMS spectrum of (–)-NRG-DM; Figure S3: <sup>1</sup>H NMR spectrum of (–)-NRG-DM (400 MHz, CDCl<sub>3</sub>); Figure S4: <sup>13</sup>C NMR spectrum of (–)-NRG-DM (100 MHz, CDCl<sub>3</sub>).

**Author Contributions:** Conceptualization, Y.-M.Z., Z.-B.G. and J.-L.Y.; methodology, Y.-M.Z. and X.-H.M.; validation, R.-R.G., X.-H.M. and Y.Z.; formal analysis, R.-R.G. and X.-H.M.; investigation, R.-R.G., X.-H.M., Y.Z., H.-Y.X. and L.Z.; resources, Z.-B.G. and J.-L.Y.; writing—original draft preparation, R.-R.G. and X.-H.M.; writing—review and editing, Y.-M.Z., Z.-B.G. and J.-L.Y.; visualization, Z.-B.G.; supervision, Y.-M.Z., Z.-B.G. and J.-L.Y.; project administration, Y.-M.Z.; funding acquisition, Z.-B.G., Y.-M.Z. and J.-L.Y. All authors have read and agreed to the published version of the manuscript.

**Funding:** This research was funded by the National Science Fund for Distinguished Young Scholars (81825021), the National Natural Science Foundation of China (81773707, 32161143019), the Youth Innovation Promotion Association of the Chinese Academy of Sciences (2020284), and the Fund of Science and Technology Commission of Shanghai Municipality (19431906000), Natural Science Foundation of Gansu Province (20JR5RA570), CAS “Light of West China” Program, and CAS Pioneer Hundred Talents Program.

**Institutional Review Board Statement:** The animal study protocol was approved by the IACUC (Institutional Animal Care and Use Committees) of Shanghai Institute of Materia Medica (permission number: 2021-02-GZB-09).

**Informed Consent Statement:** Not applicable.

**Data Availability Statement:** The data presented in this study are available upon request from the corresponding author.

**Acknowledgments:** The authors thank Yue-Lin Gu for her assistance in the construction of animal models.

**Conflicts of Interest:** The authors declare no conflict of interest. The funders had no role in the design of the study; in the collection, analyses, or interpretation of data; in the writing of the manuscript, or in the decision to publish the results.

**Sample Availability:** Samples of the compounds prepared in this article are available from the authors.

## References

1. Okifuji, A.; Skinner, M. Chapter 70—Psychological Aspects of Pain. *Curr. Ther. Pain.* **2009**, *24*, 513–518.
2. Cohen, S.P.; Vase, L.; Hooten, W.M. Chronic pain: An update on burden, best practices, and new advances. *Lancet* **2021**, *397*, 2082–2097. [[CrossRef](#)]
3. Hylands-White, N.; Duarte, R.V.; Raphael, J.H. An overview of treatment approaches for chronic pain management. *Rheumatol. Int.* **2017**, *37*, 29–42. [[CrossRef](#)] [[PubMed](#)]
4. Murphy, E.J. Acute Pain Management Pharmacology for the Patient with Concurrent Renal or Hepatic Disease. *Anaesth. Intensive Care* **2005**, *33*, 311–322. [[CrossRef](#)]
5. Cahill, C.M.; Lueptow, L.; Kim, H.; Shusharla, R.; Bishop, A.; Evans, C.J. Kappa Opioid Signaling at the Crossroads of Chronic Pain and Opioid Addiction. *Handb. Exp. Pharmacol.* **2022**, *271*, 315–350.
6. Mercadante, S.; Arcuri, E.; Santoni, A. Opioid-Induced Tolerance and Hyperalgesia. *CNS Drugs* **2019**, *33*, 943–955. [[CrossRef](#)]
7. Esposito, M.F.; Malayil, R.; Hanes, M.; Deer, T. Unique Characteristics of the Dorsal Root Ganglion as a Target for Neuromodulation. *Pain Med.* **2019**, *20* (Suppl. S1), S23–S30. [[CrossRef](#)]
8. Liem, L.; Dongen, E.V.; Huygen, F.J.; Staats, P.; Kramer, J. The Dorsal Root Ganglion as a Therapeutic Target for Chronic Pain. *Reg. Anesth. Pain Med.* **2016**, *41*, 511–519. [[CrossRef](#)]
9. Li, H.-S.; Zhao, Z.Q. Small sensory neurons in the rat dorsal root ganglia express functional NK-1 tachykinin receptors. *Eur. J. Neurosci.* **1998**, *12*, 1292–1299. [[CrossRef](#)]
10. Maljevic, S.; Lerche, H. Potassium channels: A review of broadening therapeutic possibilities for neurological diseases. *J. Neurol.* **2013**, *260*, 2201–2211. [[CrossRef](#)]
11. Bennett, D.L.; Clark, A.J.; Huang, J.; Waxman, S.G.; Dib-Hajj, S.D. The Role of Voltage-Gated Sodium Channels in Pain Signaling. *Physiol Rev.* **2019**, *99*, 1079–1151. [[CrossRef](#)] [[PubMed](#)]
12. Goodwin, G.; McMahan, S.B. The physiological function of different voltage-gated sodium channels in pain. *Nat. Rev. Neurosci.* **2021**, *22*, 263–274. [[CrossRef](#)] [[PubMed](#)]
13. Hameed, S. Nav1.7 and Nav1.8: Role in the pathophysiology of pain. *Mol. Pain.* **2019**, *15*, 1744806919858801. [[CrossRef](#)]

14. Labro, A.J.; Priest, M.F.; Lacroix, J.J.; Snyders, D.J.; Bezanilla, F. Kv3.1 uses a timely resurgent K<sup>+</sup> current to secure action potential repolarization. *Nat. Commun.* **2015**, *6*, 10173. [[CrossRef](#)] [[PubMed](#)]
15. Mara, A.; Alon, K. A Quantitative Description of Dendritic Conductances and Its Application to Dendritic Excitation in Layer 5 Pyramidal Neurons. *J. Neurosci.* **2014**, *34*, 182–196.
16. Nie, A.; Wei, C.; Meng, Z. Sodium metabisulfite modulation of potassium channels in pain-sensing dorsal root ganglion neurons. *Neurochem. Res.* **2009**, *34*, 2233–2242. [[CrossRef](#)] [[PubMed](#)]
17. Hong, J.; Qiu, J.; Wang, X.; Zhang, G. Characteristics of voltage-gated potassium currents in monosodium urate induced gouty arthritis in mice. *Inflamm. Res.* **2020**, *69*, 589–598. [[CrossRef](#)]
18. Murakoshi, H.; Trimmer, J.S. Identification of the Kv2.1 K<sup>+</sup> Channel as a Major Component of the Delayed Rectifier K<sup>+</sup> Current in Rat Hippocampal Neurons. *J. Neurosci.* **1999**, *19*, 1728–1735. [[CrossRef](#)]
19. Bocksteins, E.; Raes, A.L.; Vijver, G.V.; Bruyns, T.; Bogaert, P.V.; Snyders, D.J. Kv2.1 and silent Kv subunits underlie the delayed rectifier K<sup>+</sup> current in cultured small mouse DRG neurons. *Am. J. Physiol. Cell Physiol.* **2009**, *296*, C1271–C1278. [[CrossRef](#)]
20. Boris, V. Safronov, Ulrike Bischoff and Werner Vogel. Single voltage-gated K<sup>+</sup> channels and their functions in small dorsal root ganglion neurons of rat. *J. Physiol.* **1996**, *493*, 393–408.
21. Dhiman, N.; Bhattacharya, A. *Nardostachys jatamansi* (D.Don) DC.-Challenges and opportunities of harnessing the untapped medicinal plant from the Himalayas. *J. Ethnopharmacol.* **2020**, *246*, 112211. [[CrossRef](#)] [[PubMed](#)]
22. Gomez-Betancur, I.; Cortés, N.; Benjumea, D.; Osorio, E.; León, F.; Cutler, S.J. Antinociceptive activity of extracts and secondary metabolites from wild growing and micropropagated plants of *Reineckia alpinia*. *J. Ethnopharmacol.* **2015**, *165*, 191–197. [[CrossRef](#)] [[PubMed](#)]
23. Ahmad, M.; Yousuf, S.; Khan, M.B.; Hoda, M.N.; Ahmad, A.S.; Ansari, M.A.; Ansari, T.; Agrawal, A.K.; Islam, F. Attenuation by *Nardostachys jatamansi* of 6-hydroxydopamine-induced parkinsonism in rats: Behavioral, neurochemical, and immunohistochemical studies. *Pharmacol. Biochem. Behav.* **2006**, *83*, 150–160. [[CrossRef](#)] [[PubMed](#)]
24. Kim, D.C.; Park, J.S.; Yoon, C.S.; Kim, Y.C.; Oh, H. Nardostachin from *Nardostachys jatamansi* exerts anti-neuroinflammatory effects through TLR4/MyD88related suppression of the NF-κB and JNK MAPK signaling pathways in lipopolysaccharide-induced BV2 and primary microglial cells. *Mol. Med. Rep.* **2021**, *23*, 82. [[CrossRef](#)]
25. Yoon, C.S.; Kim, D.C.; Park, J.S.; Kim, K.W.; Kim, Y.C.; Oh, H. Isolation of Novel Sesquiterpenoids and Anti-neuroinflammatory Metabolites from *Nardostachys jatamansi*. *Molecules* **2018**, *23*, 2367. [[CrossRef](#)]
26. Yoon, C.S.; Kim, K.W.; Lee, S.C.; Kim, Y.C.; Oh, H. Anti-neuroinflammatory effects of sesquiterpenoids isolated from *Nardostachys jatamansi*. *Bioorg. Med. Chem. Lett.* **2018**, *28*, 140–144. [[CrossRef](#)]
27. Singh, M.; Khan, M.A.; T, K.Y.; Ahmad, J.; Fahmy, U.A.; Kotta, S.; Alhakamy, N.A.; Ahmad, S. Effect of *Nardostachys jatamansi* DC. On Apoptosis, Inflammation and Oxidative Stress Induced by Doxorubicin in Wistar Rats. *Plants* **2020**, *9*, 1579. [[CrossRef](#)]
28. Serafini, M.; Peluso, I.; Raguzzini, A. Flavonoids as anti-inflammatory agents. *Proc. Nutr. Soc.* **2010**, *69*, 273–278. [[CrossRef](#)]
29. Ferraz, C.R.; Carvalho, T.T.; Manchope, M.F.; Manchope, N.A.; Rasquel-Oliveira, F.S.; Fattori, V.; Casagrande, R.; Jr, W.A. Therapeutic Potential of Flavonoids in Pain and Inflammation: Mechanisms of Action, Pre-Clinical and Clinical Data, and Pharmaceutical Development. *Molecules* **2020**, *25*, 762. [[CrossRef](#)]
30. Xue, X.; Chen, Y.; Wang, Y.; Zhan, J.; Chen, B.; Wang, X.; Pan, X. Troxerutin suppresses the inflammatory response in advanced glycation end-product-administered chondrocytes and attenuates mouse osteoarthritis development. *Food Funct.* **2019**, *10*, 5059–5069. [[CrossRef](#)]
31. Hu, Y.; Gui, Z.; Zhou, Y.; Xia, L.; Lin, K.; Xu, Y. Quercetin alleviates rat osteoarthritis by inhibiting inflammation and apoptosis of chondrocytes, modulating synovial macrophages polarization to M2 macrophages. *Free Radic. Biol. Med.* **2019**, *145*, 146–160. [[CrossRef](#)] [[PubMed](#)]
32. Pinho-Ribeiro, F.A.; Zarpelon, A.C.; Fattori, V.; Manchope, M.F.; Mizokami, S.S.; Casagrande, R.; Verri, W.A. Naringenin reduces inflammatory pain in mice. *Neuropharmacology* **2016**, *105*, 508–519. [[CrossRef](#)] [[PubMed](#)]
33. Wang, Y.; Ma, G.; Huang, Z.; Zhong, X.; Xu, X.; Yuan, J. Identification of compounds in alien invasive plant *Chromolaena odorata*. *Chin. Pharm. J.* **2016**, *51*, 698–702.
34. Oyama, K.; Kondo, T. Total synthesis of flavocommelin, a component of the blue supramolecular pigment from *Commelina communis*, on the basis of direct 6-C-glycosylation of flavan. *J. Org. Chem.* **2004**, *69*, 5240–5246. [[CrossRef](#)] [[PubMed](#)]
35. Zainullin, R.A.; Kunakova, R.V.; Gareev, V.F.; Galyautdinov, I.V.; Sadretdinova, Z.R.; Muslimov, Z.S.; Odinokov, V.N. Flavanones and flavones from *Bashkir propolis*. *Chem. Nat. Compd.* **2018**, *54*, 975–977. [[CrossRef](#)]
36. Mogil, J.S. Animal models of pain: Progress and challenges. *Nat. Rev. Neurosci.* **2009**, *10*, 283–294. [[CrossRef](#)]
37. Laird, J.M.A.; Martinez-Caro, L.; Garcia-Nicas, E.; Cervero, F. A new model of visceral pain and referred hyperalgesia in the mouse. *Pain* **2001**, *92*, 335–342. [[CrossRef](#)]
38. Bean, B.P. The action potential in mammalian central neurons. *Nat. Rev. Neurosci.* **2007**, *8*, 451–465. [[CrossRef](#)]
39. Du, J.; Wang, Q.; Hu, F.; Wang, J.; Ding, H.; Gao, R.; Xiao, H.; Wang, L. Effects of estradiol on voltage-gated potassium channels in mouse dorsal root ganglion neurons. *J. Membr. Biol.* **2014**, *247*, 541–548. [[CrossRef](#)]
40. Chahine, M.; O’Leary, M.E. Regulation/modulation of sensory neuron sodium channels. *Handb. Exp. Pharmacol.* **2014**, *221*, 111–135.



41. Zhu, J.; Zang, S.; Chen, X.; Jiang, L.; Gu, A.; Cheng, J.; Zhang, L.; Wang, J.; Xiao, H. Involvement of the delayed rectifier outward potassium channel Kv2.1 in methamphetamine-induced neuronal apoptosis via the p38 mitogen-activated protein kinase signaling pathway. *J. Appl. Toxicol.* **2018**, *38*, 696–704. [[CrossRef](#)]
42. Arora, V.; Campbell, J.N.; Chung, M.K. Fight fire with fire: Neurobiology of capsaicin-induced analgesia for chronic pain. *Pharmacol. Ther.* **2021**, *220*, 107743. [[CrossRef](#)] [[PubMed](#)]
43. Hofer, M.; Hoferova, Z.; Falk, M. Brief Story on Prostaglandins, Inhibitors of their Synthesis, Hematopoiesis, and Acute Radiation Syndrome. *Molecules* **2019**, *24*, 4019. [[CrossRef](#)] [[PubMed](#)]
44. Engels, N.S.; Waltenberger, B.; Michalak, B.; Huynh, L.; Tran, H.; Kiss, A.K.; Stuppner, H. Inhibition of Pro-Inflammatory Functions of Human Neutrophils by Constituents of *Melodorum fruticosum* Leaves. *Chem. Biodivers.* **2018**, *15*, e1800269. [[CrossRef](#)] [[PubMed](#)]
45. Sheng, A.; Zhang, Y.; Li, G.; Zhang, G. Inhibitory Effects of Honokiol on the Voltage-Gated Potassium Channels in Freshly Isolated Mouse Dorsal Root Ganglion Neurons. *Neurochem. Res.* **2018**, *43*, 450–457. [[CrossRef](#)] [[PubMed](#)]
46. Zhang, Y.; Jiang, D.; Zhang, Y.; Jiang, X.; Wang, F.; Tao, J. Neuromedin U type 1 receptor stimulation of A-type K<sup>+</sup> current requires the betagamma subunits of Go protein, protein kinase A, and extracellular signal-regulated kinase 1/2 (ERK1/2) in sensory neurons. *J. Biol. Chem.* **2012**, *287*, 18562–18572. [[CrossRef](#)]
47. Clark, R.B.; Hatano, N.; Kondo, C.; Belke, D.D.; Brown, B.S.; Kumar, S.; Votta, B.J.; Votta, W.R. Voltage-gated K<sup>+</sup> currents in mouse articular chondrocytes regulate membrane potential. *Channels* **2010**, *4*, 179–191. [[CrossRef](#)]
48. Takeda, M.; Tsubo, Y.; Kitagawa, J.; Nakagawa, K.; Iwata, K.; Matsumoto, S. Potassium channels as a potential therapeutic target for trigeminal neuropathic and inflammatory pain. *Mol. Pain.* **2011**, *7*, 5. [[CrossRef](#)]
49. Lee, M.C.; Nahorski, M.S.; Hockley, J.R.F.; Lu, V.B.; Ison, G.; Pattison, L.A.; Callejo, G.; Stouffer, K.; Fletcher, E.; Brown, C.; et al. Human Labor Pain Is Influenced by the Voltage-Gated Potassium Channel K<sub>v</sub>6.4 Subunit. *Cell Rep.* **2020**, *32*, 107941. [[CrossRef](#)]
50. Leipold, E.; Liebmann, L.; Korenke, G.C.; Heinrich, T.; Heinrich, S.; Baets, J.; Ebbinghaus, M.; Goral, R.O.; Stödberg, T.; Hennings, J.C.; et al. A de novo gain-of-function mutation in *SCN11A* causes loss of pain perception. *Nat. Genet.* **2013**, *45*, 1399–1404. [[CrossRef](#)]
51. Guo, R.; Shi, A.M.; Deng, L.; Li, L.; Wang, L.; Oteng, A.B.; Wei, M.P.; Zhao, Z.H.; Hooiveld, G.; Zhang, C.; et al. Flavonoid-Like Components of Peanut Stem and Leaf Extract Promote Sleep by Decreasing Neuronal Excitability. *Mol. Nutr. Food Res.* **2021**, *66*, e2100210. [[CrossRef](#)] [[PubMed](#)]